POLITECNICO
MILANO 1863

SCUOLA DI INGEGNERIA INDUSTRIALE
E DELL'INFORMAZIONE

Executive Summary of the Thesis

A Model for Meltwater Infiltration and Refreezing in Snow under Non-Isothermal Conditions

Laurea Magistrale in Mathematical Engineering - Ingegneria Matematica

Author: Camilla Crippa

Advisor: Prof. Alessio Fumagalli

Co-advisor: Prof.ssa Anna Scotti

Academic year: 2022-2023

1. Introduction

In this thesis, the focus is on understanding the flow of meltwater through snow. Enhancing our comprehension of the intricate dynamics of water flow within snow is imperative for evaluating and minimizing the hazards associated with avalanches, as well as grasping the mechanisms driving glacier movement [3]. Infiltrating water, for example, functions as a lubricant, easing the movement of the snowpack or glacier as it slides over the bedrock beneath.

The aim is to model the complex interaction between meltwater infiltration and non-equilibrium thermodynamics of ice-melt phase change at the Darcy scale. In particular, the modeling of the thermal budget is grounded in the work put forth by [2].

The model presented in this work consists of the Richards' equation for infiltration, and evolution equations for ice and water temperature fields that account for the thermal budget resulting from melt refreezing. Additionally, the model considers variations in porosity, as already explored in [5]. An iterative coupling is designed between the fluid-mechanics and thermodynamics macroprocesses, where the system of equations is numerically solved by employing the Mixed Finite Element Method for Richards' equation and the Finite Volume Method discretization scheme for the thermal budget equations. Numerical simulations, conducted on snowpacks with different initial dryness levels and physical setups, present the model's application. The Python libraries *PorePy* [4] and *PyGeoN* [1] are employed for implementation.

2. The Model

The microscopic structure of snow is well-known to include ice crystals, often called *grains*. These grains, rather than filling the entire volume, create, when packed, void spaces within the structure, categorizing snow as a porous medium.

In the opening section of our thesis we introduce the concept of porous media. Specifically, since we deal with a two-phase flow scenario where the void space accommodates both water and air simultaneously, we employ the *Richards' assumption* [6] for the air phase to derive Richards' equation.

Modeling the infiltration of water into a snowpack presents a challenge due to the fact that the infiltrating phase, water, shares identical chemical properties with the medium it infiltrates, namely ice. The only distinguishing factor be-

tween them is their physical state.
Infiltration typically manifests a heterogeneous nature, with the formation of fingers resulting from both property heterogeneities and the intrinsic instability of the meltwater front. This aspect can be modeled, as proposed by [5], by adding a fourth-order term in saturation to the Richards' equation. However, in this work, we overlook this aspect, focusing solely on the fluid-dynamic/thermal coupling and consequently utilizing the classical version of the equation.
Thermodynamically, the model includes a non-isothermal condition, accounting for the influence of latent heat release during phase change and its impact on the thermal energy balance of the snowpack. This thesis adopts a dual-temperature field framework, specifically incorporating a *local thermal non-equilibrium* (LTNE) condition.
As mentioned earlier, the snowpack is treated as a porous medium consisting of water, air, and ice. In this context, water acts as the wetting fluid, air as the nonwetting fluid, and ice as the solid matrix. The unknowns in the model are defined as volume-averaged quantities over a REV and include:

- Porosity $\phi(\mathbf{x}, t)$,
- Water Saturation $S(\mathbf{x}, t)$,
- Hydraulic pressure of water phase $\psi(\mathbf{x}, t)$,
- Darcy velocity of melt infiltration $\mathbf{q}(\mathbf{x}, t)$,
- Ice temperature $T_i(\mathbf{x}, t)$,
- Water temperature $T_w(\mathbf{x}, t)$.

2.0.1 Equations for Infiltration Mechanics and Mass Conservation

The ice mass conservation equation can be written as:

$$\rho_i \frac{\partial(1-\phi)}{\partial t} = -\rho_i R_m W_{SSA}(T_{int} - T_{melt}), \quad (1)$$

while the water mass conservation equation reads:

$$\rho_w \left(\frac{\partial \theta(\psi)}{\partial t} + \boldsymbol{\nabla} \cdot \mathbf{q} \right) = \rho_i R_m W_{SSA}(T_{int} - T_{melt}), \quad (2)$$

where ρ_α is the constant density for phase α ($\alpha = i, w$), $\theta = \phi S$, R_m is a constant depending on thermodynamic quantities, $W_{SSA}(S, \phi)$ is the *wet specific area* and T_{int} denotes a weighted average between the temperatures of ice and water.
The meltwater Richards' flux follows:

$$\mathbf{q} = -K_s(\phi) k_r(\psi) \boldsymbol{\nabla} \Pi(\psi) \quad (3)$$

where $k_r(\psi)$ is the water relative hydraulic conductivity, $K_s(\phi)$ is the snow hydraulic conductivity in the fully saturated case and $\Pi(\psi) = \psi + z$ is the overall flow potential.
In particular, to define the expressions of $\theta(\psi)$ and $k_r(\psi)$ we employ the Van Genuchten model:

$$\theta(\psi) = \begin{cases} \theta_r + \dfrac{\theta_s - \theta_r}{[1 + (-\alpha\psi)^n]^{\frac{n-1}{n}}} & \text{if } \psi \leq 0 \\ \theta_s & \text{if } \psi > 0 \end{cases}$$

$$k_r(\psi) = \Theta(\psi)^{\frac{1}{2}} \left[1 - \left(1 - \Theta(\psi)^{\frac{1}{m}} \right)^m \right]^2$$

In this study, we exclusively examined a specific type of snow characterized by relatively small grains, as detailed in [3]. The parameters α and n are uniquely determined by the grain size and its associated density. For the selected grain size, α and n are regarded as "extreme values" for the chosen model. In fact, the shapes of $\theta(\psi)$ and $k_r(\psi)$ are highly steep within a specific interval for ψ.
Given a specified rectangular region of a two-dimensional space denoted as Ω, the boundary conditions pertaining to Richards' equation for this model are the following:

$$\begin{aligned} &\mathbf{q} \cdot \mathbf{n} = 0 && \text{on } \Gamma_l \cup \Gamma_b \\ &\psi = \psi_{top} > 0 && \text{on } \Gamma_t \end{aligned}$$

where $\Gamma_t, \Gamma_b, \Gamma_l$ represent the upper, lower and lateral boundary portion respectively. The condition on Γ_t simulates a continuous source of full saturation intended to infiltrate into the snowpack. Regarding initial conditions, we set $\psi(\mathbf{x}, 0) = \psi_0$, $\phi(\mathbf{x}, 0) = \phi_0$.

2.0.2 Equations for Temperatures and Phase Change

The temperature evolution equations for ice and water phases read as follows:

$$\rho_i c_i \frac{\partial[(1-\phi)T_i]}{\partial t} - \boldsymbol{\nabla}\cdot(K_i(1-\phi)\boldsymbol{\nabla}T_i) = -\alpha_i C, \tag{4}$$

$$\rho_w c_w \left[\frac{\partial(\phi S T_w)}{\partial t} + \boldsymbol{\nabla}\cdot(\mathbf{q}T_w)\right] + -\boldsymbol{\nabla}\cdot(K_w\phi S\boldsymbol{\nabla}T_w) = -\alpha_w C \tag{5}$$

where c_α, k_α are constants, $\alpha_\alpha(T_i, T_w, T_{int})$ accounts for phase change and
$C = \rho_w L_{sol} R_m W_{SSA}(T_{int} - T_{melt})$.
Consistent with the previously mentioned boundary partitioning, the boundary conditions are the following:

$$\begin{aligned}
&D_i(1-\phi)\boldsymbol{\nabla}T_i\cdot\mathbf{n} = 0, && \text{on } \Gamma_l\\
&T_i = T_{melt}, && \text{on } \Gamma_t\\
&T_i = T_{i,b}, && \text{on } \Gamma_b
\end{aligned}$$

$$\begin{aligned}
&(D_w\phi S\boldsymbol{\nabla}T_w - \mathbf{q}T_w)\cdot\mathbf{n} = 0 && \text{on } \Gamma_l\\
&T_w = T_{melt} && \text{on } \Gamma_t\\
&(D_w\phi S\boldsymbol{\nabla}T_w - \mathbf{q}T_w)\cdot\mathbf{n} = 0 && \text{on } \Gamma_b
\end{aligned}$$

Regarding initial conditions, we set $T_i(\mathbf{x}, 0) = T_{i,0}$, $T_w(\mathbf{x}, 0) = T_{w,0}$.

3. Discretization Methods

The methods employed for the temporal and spatial discretization of the two classes of equations are briefly presented.

3.1. Richards' equation discretization

To numerically solve Richards' equation (2), (3) we first derive its weak formulation and then proceed with temporal discretization using the Backward Euler approach. In particular, the right-hand side is treated implicitly; indeed, it depends on S^{n+1}, ϕ^{n+1} and T_{int}^{n+1}, which are obtained and corrected iteratively.
Richards' equation is a nonlinear partial differential equation and, to address its nonlinearities, we exploit the L-scheme method. Finally, concerning space discretization, we employ the Mixed Finite Element method [7], which is well-suited for triangular meshes and efficient in addressing problems with significant variations in the coefficients' magnitudes. The chosen spaces for pressure and flux are $\mathbb{P}^0$ and $\mathbb{RT}^0$ respectively.

3.2. Porosity equation discretization

The equation for porosity (1) is an ordinary differential equation, discretized in time using the Backward Euler method. Similar to the previous case, the right-hand side is treated implicitly by iteratively correcting S^{n+1} and T_{int}^{n+1}.

3.3. Temperature equations discretization

The equations for the two thermodynamic fields (4), (5) are discretized in time employing an implicit scheme for the diffusive and transport terms. Simultaneously, the reaction term is adjusted iteratively, promoting the coupling between the two equations.
Regarding space discretization, it is accomplished using the Finite Volume method [7]. Specifically, for the diffusive term, the *MPFA* method is used, while for the transport term in the water equation, the *Upwind* scheme is adopted. The equation is initially integrated over a control volume, and then the integral of the divergence term is expressed as the sum of numerical fluxes, defined differently based on the chosen method. The final finite volume system is built by summing over all control volumes. The solution of the system for each time step is the couple $(\underline{T}_i^{n+1}, \underline{T}_w^{n+1}) \in \mathbb{V}^h \times \mathbb{V}^h$, where $\mathbb{V}_h = \{v \in L^2(\Omega) : v|_K = \text{const } \forall K \in \mathcal{T}_h\}$ and $\mathcal{T}_h$ is the chosen triangulation.

4. Details of the implementation

Here are some additional details for the numerical implementation.

4.1. Domain and grid

The aim is to implement the model in a physical domain in two dimensions, specifically representing a thin column extracted from a snowpack. In particular, we consider $\Omega = (0, 0.2)$ m $\times (0, 1)$ m.
The domain is discretized using a structured triangle grid, where the number of triangular cells in the vertical z dimension is five times greater than the number of cells in the horizontal x direction. The analytical expressions for the boundaries are presented below:

$$\Gamma_t = \{(x,z) \in \partial\Omega \,|\, z = 1\},$$
$$\Gamma_b = \{(x,z) \in \partial\Omega \,|\, z = 0\},$$
$$\Gamma_l = \{(x,z) \in \partial\Omega \,|\, x = 0 \vee x = 0.2\}.$$

4.2. Coupling Strategy

The coupling strategy between the two macro-processes is addressed in Algorithm 1.

Algorithm 1 Pseudocode

Initialization
for n in $0, ..., N_{ts}$ **do**
  Definition of $L^n = \max_{\psi^n<0} \theta'^n(\psi^n)$
  Definition of time-dependent rhs for Darcy and mass conservation equation
  for j in $0, ..., J$ **do**
    for k in $0, ..., K$ **do**
      Solve Richards using $S^{n+1}_{k,j}$, $\phi^{n+1}_{k,j}$, $T^{n+1}_{int,j}$
      for m in $0, ..., M$ **do**
        Update: $S^{n+1}_{m+1,j+1,k+1} = f(\psi^{n+1}_{k+1}, \phi^{n+1}_{m,j+1,k+1})$
        Update: $\phi^{n+1}_{m+1,j+1,k+1} = g(\phi^{n+1}_{m,j+1,k+1}, S^{n+1}_{m+1,j+1,k+1}, T^{n+1}_{int,j})$
      end for
      # We have $S^{n+1}_{k+1,j+1}, \phi^{n+1}_{k+1,j+1}$
    end for
    # We have q^{n+1}_{j+1}, ψ^{n+1}_{j+1}, S^{n+1}_{j+1}, ϕ^{n+1}_{j+1}
    Solve Thermodynamics using the above quantities and $T^{n+1}_{int,j}$
    # We have $T^{n+1}_{i,j+1}$, $T^{n+1}_{w,j+1}$
    Update: $T^{n+1}_{int,j+1} = h(T^{n+1}_{i,j+1}, T^{n+1}_{w,j+1})$
  end for
  # We have q^{n+1}, ψ^{n+1}, S^{n+1}, ϕ^{n+1}, T^{n+1}_i, T^{n+1}_w, T^{n+1}_{int}
  Export q^{n+1}, ψ^{n+1}, S^{n+1}, ϕ^{n+1}, T^{n+1}_i, T^{n+1}_w, T^{n+1}_{int}
end for

The L-scheme for the Richards' equation, whose L parameter is time-dependent, is solved in the k-loop. The coupling among pressure, flux, porosity and the two temperatures is enforced iteratively in the j-loop. Moreover, an additional w-loop is implemented to iteratively update the values of S and ϕ. The functions f, g, h are defined in the thesis.

5. Numerical Results

Here some key results from 2D simulations are presented.

5.1. Initially dry snowpack

When considering a snowpack with an initial high level of dryness (i.e., selecting ψ_0 such that S_0 is on the order of 10^{-3}), complete refreezing and absence of infiltration are observed. Indeed, for this value of ψ_0, we obtain an extremely low value for $k_r(\psi)$, resulting in a remarkably low permeability of the medium from the outset. Figure 1 shows a sudden decrease in saturation and porosity occurring at a depth of 50 cm, indicating refreezing. Just beneath the surface, there's a change in the scenario: saturation initially declines similarly to the previously analyzed case but later suggests an increasing trend. Meanwhile, porosity experiences an initial sharp decrease followed by further reduction.

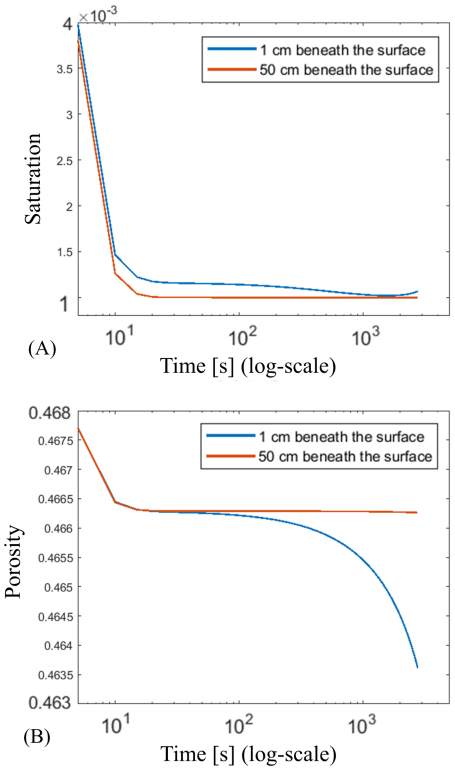

Figure 1: (A) Depth-averaged saturation, (B) Depth-averaged porosity over time.

Regarding temperatures, ice experiences heat

diffusion from the overlying water source. Over time, the ice layer near Γ_t slowly approaches the melting temperature. The temperature of ice for the upper 10 cm of snowpack for $t = 1955$ s is reported in Figure 2:

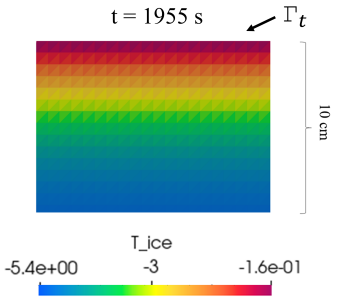

Figure 2: Ice temperature experiences heat diffusion.

According to [5], infiltration might be observable in a matter of days. However, this study lacks the computational resources to simulate this extensive time frame.

5.2. Initially wet snowpack

To induce infiltration, the initial condition for hydraulic pressure is set to $\psi_0 = -0.22$ m, corresponding to $S_0 \approx 0.223$. In this scenario, the value of $k_r(\psi)$ is relatively high from the beginning. Infiltration occurs, accompanied by the initial refreezing of a portion of the water initially present in the snowpack.

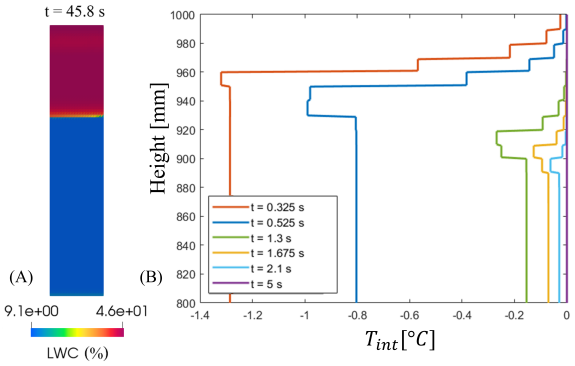

Figure 3: (A) LWC, (B) T_{int} against the quota z for six time instants.

Infiltration for $t = 45.8$ s is shown in Figure 3.A, where the *liquid water content* (LWC) is expressed as the percentage associated with the moisture content $\theta = S\phi$. Owing to the heat released by the substantial presence of water within the domain, the temperature of the ice approaches the melting point during the initial time period. As shown in Figure 3.B, we notice an undershoot in the interface temperature before reaching equilibrium, which is notably located at the infiltration front and entails a further decrease in porosity. Over time, we witness a decrease in both the intensity and quota of the undershoot. Moreover, in regions where the medium is completely saturated with water, the interface temperature reaches the melting point more rapidly than in the rest of the domain. Graphical illustrations supporting the arguments are provided in the thesis.

5.3. Heterogeneous conditions

Other interesting physical setups have been implemented in the case of initially wet snowpack. Three different simulated LWC configurations for three different time instants are provided in Figure 4.
Figure 4.A depicts the onset of infiltration in the scenario of a discretely distributed pressure source at Γ_t. In particular, we impose $\psi_{top} = 1$ on Γ_t^A and $\psi_{top} = 0$ on Γ_t^B, where

$$\Gamma_t^A = \{(x, z) \in \Gamma_t \,|\, x \in [0.04, 0.06] \vee [0.14, 0.16]\},$$
$$\Gamma_t^B = \Gamma_t \backslash \Gamma_t^A.$$

Upon water entering the domain, infiltration occurs both vertically and horizontally, saturating the width of the domain within the initial centimeters. Notably, the infiltration process is more pronounced at the abscissa where the source is located. However, as time progresses, the profile of the front gradually loses its distinctive shape. The same line of reasoning employed in Section 5.2 regarding temperatures and phase change can be applied in this scenario, with the only difference being the shape of the undershoot, which is consistent with that of the infiltration front. Figure 4.B pertains to a case where warm water is injected into the domain at $t = 0$ s, creating an initial fully saturated *bubble* inside the domain. Under the influence of gravity, the bubble begins its downward motion. However, its movement is not restricted to the vertical direction, but it also displays a notable diffusive behavior. Within the internally saturated region, results show that porosity attains its maximum value throughout the snowpack.

The instantaneous injection, initially endowed with a certain pressure, accelerates the ice's approach to the melting point, limiting the refreezing in that area. Finally, Figure 4.C refers to a scenario where the domain is initially composed of zones characterized by different permeabilities. Especially remarkable is water's tendency to follow paths with higher permeability, facilitating infiltration in these areas. Conversely, regions with closer-to-impermeable characteristics tend to be initially avoided.

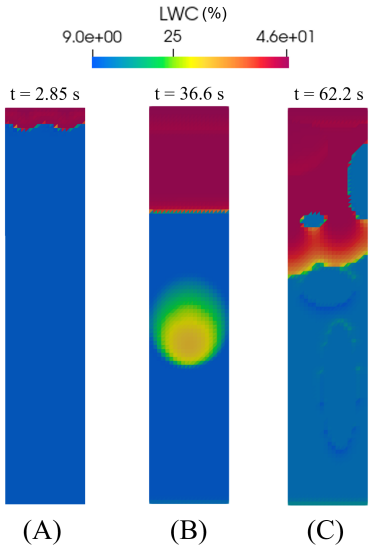

Figure 4: (A) LWC from discrete pressure source, (B) LWC from instantaneous injection, (C) LWC from grain-induced heterogeneity.

6. Conclusions

A deeper understanding of water flow in snow is vital for avalanche risk assessment and glacier movement comprehension. As a matter of fact, infiltrating water can lubricate, aiding snowpack or glacier sliding. In this work, we presented a model aimed at managing the interplay between fluid-dynamics and thermodynamics during meltwater flow in snow. The approach to the numerical resolution of this model involves an intricate iterative coupling strategy, integrating Richards' equation for infiltration with an ODE for porosity and two advection-diffusion-reaction equations for temperatures and phase change. Various numerical tests have been conducted to evaluate infiltration and phase change thermodynamics, particularly refreezing-induced solidification. Notably, the initial dryness level significantly influences the dynamics of the infiltration process. The study suggests improving the model by extending Richards'equation with an extra term, which could significantly advance understanding meltwater transport and its instabilities at the front. Moreover, the inclusion of variable ice density to account for a compressible snowpack could further improve the reproduction of the observed phenomenon. Future developments may finally refine the coupling strategy for improved convergence efficiency in terms of time step size.

References

[1] Alessio Fumagalli Anna Scotti Enrico Ballini, Wietse Boon. Pygeon: a python package for geo-numerics. url https://github.com/compgeo-mox/pygeon, 2022.

[2] T Heinze. A multi-phase heat transfer model for water infiltration into frozen soil. *Water Resources Research*, 57(10):e2021WR030067, 2021.

[3] Takafumi Katsushima, Satoru Yamaguchi, Toshiro Kumakura, and Atsushi Sato. Experimental analysis of preferential flow in dry snowpack. *Cold Regions Science and Technology*, 85:206–216, 2013.

[4] Berge R. Fumagalli A. Starnoni M. Stefansson I. Varela J. Berre I. Keilegavlen, E. Porepy: an open-source software for simulation of multiphysics processes in fractured porous media. *Computational Geosciences*, 25:243–265, 10 2021.

[5] Adrian Moure, Nathan Jones, Joshua Pawlak, Colin Meyer, and Xiaojing Fu. A thermodynamic nonequilibrium model for preferential infiltration and refreezing of melt in snow. *Water Resources Research*, 59(5):e2022WR034035, 2023. e2022WR034035 2022WR034035.

[6] G.F. Pinder and M.A. Celia. *Subsurface Hydrology*. Wiley, 2006.

[7] Alfio Quarteroni. *Numerical Models for Differential Problems*, volume 1. Springer Milano, 2 edition, 4 2014.